Experimental and Computational Investigation of Gas-Phase Reaction of Chlorine with *n*-Propanol: Observation of Chloropropanol Conformational Isomerization at Room Temperature

T. Yamanaka and M. Kawasaki*

Department of Molecular Engineering, Kyoto University, Kyoto 615-8510, Japan

M. D. Hurley and T. J. Wallington*

Ford Motor Company, P.O. Box 2053, Dearborn, Michigan 48121-2053

L. Xiao and W. F. Schneider*

Department of Chemical and Biomolecular Engineering, University of Notre Dame, Notre Dame, Indiana 46556

Received: December 18, 2007; In Final Form: January 15, 2008

FTIR smog chamber techniques were used to measure $k(Cl+n\text{-}C_3H_7OH) = (1.74 \pm 0.15) \times 10^{-10}$ and $k(Cl+CH_2ClCH_2CH_2OH) = (7.54 \pm 0.73) \times 10^{-11}$ cm^3 molecule^{-1} s^{-1} in 700 Torr of N_2 at 296 K. The reaction of Cl with n-C_3H_7OH gives CH_3CH_2CHOH, CH_3CHCH_2OH, and $CH_2CH_2CH_2OH$ radicals in yields of 60 ± 5, 25 ± 8, and 15 ± 3%, respectively. Neither $CH_3CH_2CHClOH$ nor $CH_3CHClCH_2OH$ is available commercially, and infrared spectra for the three chlorides $CH_3CH_2CHClOH$, $CH_3CHClCH_2OH$, and $CH_2ClCH_2CH_2OH$ were calibrated experimentally. MP2/6-31G(d,p) calculations were used to corroborate the experimental vibrational assignments. Analysis reveals that each geometric isomer possesses several structurally and spectroscopically distinct conformers arising from intramolecular hydrogen bonding and, in the case of $CH_3CH_2CHClOH$, negative hyperconjugation. These conformers interchange slowly enough to be distinguished within the room-temperature vibrational spectrum. The experimentally observed vibrational spectra are well described by a Boltzmann-weighted superposition of the conformer spectra. As is typical of α-halogenated alcohols, $CH_3CH_2CHClOH$ readily decomposes heterogeneously to propanal and HCl.

1. Introduction

Concerns over climate change and energy security have led to increased interest in the use of renewable biofuels in the automotive fuel pool. The principal biofuels under consideration are methyl esters of long chain fatty acids (e.g., $C_{15}H_{31}C(O)OCH_3$ from palmitic acid, $C_{17}H_{35}C(O)OCH_3$ from stearic acid) for blending in diesel and alcohols (e.g., C_2H_5OH, C_3H_7OH, and C_4H_9OH) for blending in gasoline. Prior to the large scale use of such biofuels, it is desirable to have a detailed understanding of their environmental impact. In smog chamber studies of the atmospheric oxidation mechanisms of organic compounds, it is often advantageous to employ Cl atom initiated oxidation in place of the OH radical initiated oxidation which occurs in the atmosphere. The mechanisms of the reactions of Cl atoms with organic compounds are often similar to those of the analogous reactions of OH radicals. It is generally more convenient in the laboratory to generate Cl atoms than OH radicals.

Facilitation of the design and interpretation of smog chamber studies of the Cl atom initiated oxidation of biofuels requires knowledge of the kinetics and mechanisms of the Cl atom reactions and spectroscopy of products. While there have been several kinetic studies of the reaction of Cl atoms with *n*-propanol,[1,2,3,4,5] there has only been one study of the reaction mechanism.[6] To improve our understanding of the reactions of Cl atoms with alcohols in general and the atmospheric chemistry of *n*-propanol in particular we have conducted a smog chamber FTIR study of the kinetics and mechanism of reaction 1.

$$Cl + CH_3CH_2CH_2OH \rightarrow CH_3CH_2CHOH + HCl \quad (1a)$$

$$Cl + CH_3CH_2CH_2OH \rightarrow CH_3CHCH_2OH + HCl \quad (1b)$$

$$Cl + CH_3CH_2CH_2OH \rightarrow CH_2CH_2CH_2OH + HCl \quad (1c)$$

Abstraction of the hydrogen in the −OH group in *n*−propanol is endothermic by 6.3 kJ mol^{-1} [7] and is not significant at ambient temperature. We report measurements of k_1, k_{1a}/k_1, k_{1b}/k_1, and k_{1c}/k_1 at 296 K and discuss these results with respect to the literature data. As is common for 1-chloroalcohols, $CH_3CH_2CHClOH$ is found to decompose readily in the smog chamber in a fashion consistent with a heterogeneous decomposition pathway.

To establish the product identities and reaction 1 branching ratios, vibrational spectra of $CH_3CH_2CHClOH$, $CH_3CHClCH_2OH$, and $CH_2ClCH_2CH_2OH$ were determined experimentally at room temperature and compared to predictions from ab initio quantum mechanical calculations. As has been observed for 2-chloroethanol[8] and 2-fluoroethanol,[9] each of the chloropro-

* Corresponding authors: E-mail: kawasaki@moleng.kyoto-u.ac.jp; wschneider@nd.edu; twalling@ford.com.

10.1021/jp711882c CCC: $40.75
Published on Web 03/11/2008

panols exhibits several spectroscopically distinct and stable conformational isomers arising from strong intramolecular nonbonded interactions and negative hyperconjugation[10] associated with the electronegative Cl and OH substituents. The observed vibrational spectra can be accounted for by a Boltzmann-weighted linear combination of the individual conformer spectra, and in the cases of $CH_3CH_2CHClOH$ and $CH_3CHClCH_2OH$, the contributions of individual conformers are clearly distinguished in the observed spectra.

2. Experimental and Computational Methods

2.1. Experimental Details. Experiments were performed in a 140-L Pyrex reactor interfaced to a Mattson Sirus 100 FTIR spectrometer.[11] The reactor was surrounded by 22 fluorescent blacklamps (GE F15T8-BL) which were used to photochemically initiate the experiments. Cl atoms were generated from the photolysis of molecular chlorine in 700 Torr of N_2 diluent at 296 ± 2 K. The branching ratios for reaction channels 1a, 1b, and 1c were determined by measuring the formation of 1-, 2-, and 3-chloro-1-propanol following the UV irradiation of $CH_3CH_2CH_2OH/Cl_2/N_2$ mixtures. Chloropropanols are formed as the result of photochemical chain chlorination reactions.

$$Cl_2 + h\nu \rightarrow 2Cl \quad (2)$$

$$CH_3CH_2CHOH + Cl_2 \rightarrow CH_3CH_2CHClOH + Cl \quad (3)$$

$$CH_3CHCH_2OH + Cl_2 \rightarrow CH_3CHClCH_2OH + Cl \quad (4)$$

$$CH_2CH_2CH_2OH + Cl_2 \rightarrow CH_2ClCH_2CH_2OH + Cl \quad (5)$$

The rate of reaction 1 was studied using relative rate techniques. In the relative rate experiments the following reactions take place:

$$Cl + CH_3CH_2CH_2OH \rightarrow \text{products} \quad (1)$$

$$Cl + CH_3CH_2CH_2OH \rightarrow CH_3CH_2CHOH + HCl \quad (1a)$$

$$Cl + CH_3CH_2CH_2OH \rightarrow CH_3CHCH_2OH + HCl \quad (1b)$$

$$Cl + CH_3CH_2CH_2OH \rightarrow CH_2CH_2CH_2OH + HCl \quad (1c)$$

$$Cl + \text{reference} \rightarrow \text{products} \quad (6)$$

It can be shown that

$$Ln\left(\frac{[CH_3CH_2CH_2OH]_{to}}{[CH_3CH_2CH_2OH]_t}\right) = \frac{k_1}{k_6} Ln\left(\frac{[\text{reference}]_{t_0}}{[\text{reference}]_t}\right) \quad (7)$$

where $[CH_3CH_2CH_2OH]_{to}$, $[CH_3CH_2CH_2OH]_t$, $[\text{reference}]_{to}$ and $[\text{reference}]_t$ are the concentrations of $CH_3CH_2CH_2OH$ and reference compound at times t_0 and t, and k_1 and k_6 are the rate constants for reactions 1 and 6. Plots of $\ln[CH_3CH_2CH_2OH]_{to}/[CH_3CH_2CH_2OH]_t$) versus $\ln([\text{reference}]_{t_0}/[\text{reference}]_t)$ should be linear, pass through the origin, and have a slope of k_1/k_6.

Concentrations of reactants and products were monitored by FTIR spectroscopy using an analytical path length of 27 m. In the kinetic experiments IR spectra were derived from 32 co-added interferograms using a spectral resolution of 0.25 cm^{-1} with a total data acquisition time of 90 s. In the mechanistic experiments IR spectra were derived from 8 co-added interferograms using a spectral resolution of 1.0 cm^{-1} with a total data acquisition time of 11 s. Unless stated otherwise, the quoted uncertainties are 2 standard deviations from least-squares regression analyses. Reagents were obtained from commercial sources at purities >99%. The $CH_3CH_2CH_2OH$ sample was subjected to freeze−pump−thaw cycling to remove volatile impurities below use. Ultrahigh purity (>99.994%) N_2 diluent gas was used as received. In smog chamber experiments, unwanted loss of reactants and products via photolysis and heterogeneous reactions has to be considered. Control experiments were performed in which product mixtures obtained after UV irradiation were allowed to stand in the dark in the chamber for 1 h. With the exception of 1-chloro-1-propanol, there was no observable (<2%) loss of reactants or products, showing that unwanted heterogeneous reactions are not a significant complication over the time scale of the present experiments.

2.2. Computational Details. Structures of geometric and conformational isomers were determined through geometry optimizations at the second-order Møller−Plesset level (MP2), using a 6-31G** basis and the Gaussian 03 code.[12] The identities of all minima and transition states were confirmed through vibrational analysis using finite differencing at this same level of theory. The calculated harmonic vibrational frequencies were scaled by 0.94 to correct for systematic deviations[13] from the observed anharmonic modes. To facilitate comparisons with observed spectra, synthetic spectra for each geometric isomer were generated by Boltzmann weighting the individual conformers using the calculated MP2/6-31G** electronic and zero-point energies and broadening the individual bands with a Lorentzian distribution[14]

$$f(\nu) = \frac{\sum_{\text{conf}} \left\{ \exp(-\Delta E_{\text{conf}}/k_B T) \sum_{i=1}^{3n-6} I_i^{\text{conf}} \frac{1}{\pi} \left[\frac{\gamma}{(\nu - \nu_i^{\text{conf}})^2 + \gamma^2} \right] \right\}}{\sum_{\text{conf}} \exp(-\Delta E_{\text{conf}}/k_B T)} \quad (8)$$

Here ΔE_{conf} is the conformer energy relative to the most stable conformer, ν_i^{conf} and I_i^{conf} are the $3n - 6$ normal-mode frequencies and intensities, respectively, in each conformer, and γ is the half-width at half-maximum of the broadened band, set to 4 cm^{-1} here.

3. Results

3.1. Relative Rate Study of $k(Cl+C_3H_6)/k(Cl+C_2H_4)$. As a preliminary exercise prior to measuring $k(Cl+CH_3CH_2CH_2OH)$ a series of experiments were performed to measure the rate constant ratio $k(Cl+C_3H_6)/k(Cl+C_2H_4)$.

$$Cl + C_3H_6 \rightarrow \text{products} \quad (9)$$

$$Cl + C_2H_4 \rightarrow \text{products} \quad (10)$$

Experiments were conducted using mixtures of 7.05−23.1 mTorr C_3H_6, 7.20−8.23 mTorr C_2H_4, and 162−204 mTorr Cl_2 in 700 Torr of either N_2, or air, diluent. Figure 1 shows a plot of the observed loss of C_3H_6 versus that for C_2H_4 in these experiments. There was no discernible difference in the results obtained using air or N_2 diluent. The line through the data in Figure 1 is a linear least-squares fit which gives a slope of $k_9/k_{10} = 2.87 \pm 0.14$. This result can be compared to indirect determinations of $k_9/k_{10} = 2.30 \pm 0.09$ derived from work by Atkinson and Aschmann[15] in 735 Torr of air, $k_9/k_{10} = 2.66 \pm 0.19$ derived from work by Wallington et al.[16] in 740 Torr of air, and $k_9/k_{10} = 2.79 \pm 0.20$ derived from work by Kaiser and Wallington[17,18] in 700 Torr of N_2 diluent. The value of k_9/k_{10} measured directly in the present work is indistinguishable from

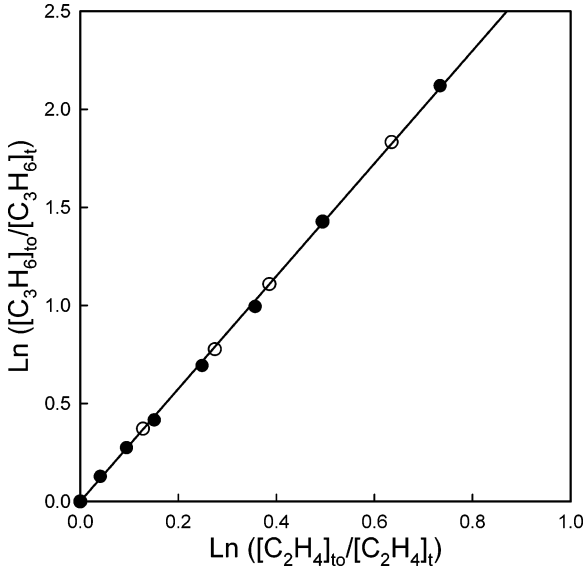

Figure 1. Loss of C_3H_6 versus C_2H_4 in the presence of Cl atoms in 700 Torr of N_2 (open symbols) or air (filled symbols) diluent at 296 ± 2 K.

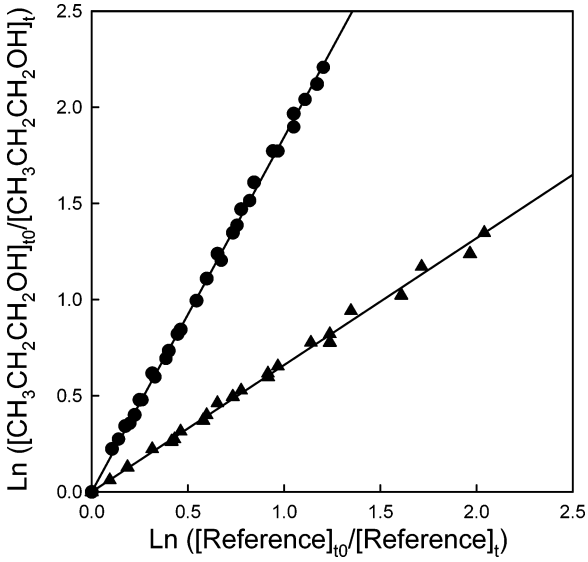

Figure 2. Loss of $CH_3CH_2CH_2OH$ versus C_2H_4 (circles) and C_3H_6 (triangles) in the presence of Cl atoms in 700 Torr of N_2 at 296 ± 2 K.

previous indirect (via the intermediacy of either *n*-butane or ethane references) measurements at Ford but somewhat higher than that derived from the data of Atkinson and Aschmann.[15]

3.2. Relative Rate Study of *k*(Cl+$CH_3CH_2CH_2OH$). The rate of reaction 1 was measured relative to reactions 9 and 10

$$Cl + CH_3CH_2CH_2OH \rightarrow \text{products} \qquad (1)$$

Reaction mixtures consisted of 42.2−87.3 mTorr of $CH_3CH_2CH_2OH$, 1.47−7.90 mTorr of reference, and 146−235 mTorr of Cl_2 in 700 Torr total pressure of N_2 diluent. The observed loss of $CH_3CH_2CH_2OH$ versus those of the reference compounds is shown in Figure 2. Linear least-squares analysis of the data in Figure 2 gives $k_1/k_9 = 0.66 \pm 0.04$ and $k_1/k_{10} = 1.84 \pm 0.13$. Taking a ratio of these ratios provides an indirect measure of $k_9/k_{10} = 2.79 \pm 0.26$ which is consistent with the direct measurement of $k_9/k_{10} = 2.87 \pm 0.14$ discussed in section 3.1.

Using $k_9 = 2.67 \times 10^{-10}$ (average of literature data given in Table 2 of Ezell et al.[19]) and $k_{10} = 9.29 \times 10^{-11}$ cm^3 molecule^{-1} s^{-1}[18] to place our relative rate measurements on an absolute basis gives $k_1 = (1.76 \pm 0.11) \times 10^{-10}$ and $(1.71 \pm 0.12) \times 10^{-10}$ cm^3 molecule^{-1} s^{-1}.

TABLE 1: Reported Values of k(Cl+*n*-C_3H_7OH) near 298 K

k_1 (cm^{3}molecule^{-1}s^{-1})	temp (K)	technique [a]	ref
$(1.49 \pm 0.12) \times 10^{-10}$ [b]	295	RR [C_2H_6]	1
$(1.53 \pm 0.07) \times 10^{-10}$ [b]	298	RR [cyclohexane]	2
$(1.69 \pm 0.20) \times 10^{-10}$ [b]	298	RR [C_2H_6]	6
$(1.64 \pm 0.14) \times 10^{-10}$ [b]	295	RR [C_3H_8]	3
$(1.56 \pm 0.12) \times 10^{-10}$ [b]	295	RR [cyclohexane]	3
$(1.71 \pm 0.11) \times 10^{-10}$	295	PLP-LIF	4
$(1.53 \pm 0.12) \times 10^{-10}$	298	LP-RF	5
$(1.74 \pm 0.15) \times 10^{-10}$	296	RR [C_2H_4, C_3H_6]	this work

[a] RR, relative rate using [reference compound(s)]; PLP-LIF, pulsed laser photolysis laser induced fluorescence; LP-RF, laser photolysis resonance fluorescence. [b] Taken from IUPAC evaluation.[25]

Indistinguishable values of k_1 were obtained using the two different references. We choose to cite a final value which is the average together with error limits which encompass the extremes of the individual determinations; $k_1 = (1.74 \pm 0.15) \times 10^{-10}$ cm^3 molecule^{-1} s^{-1}. As shown in Table 1, this result is in excellent agreement with previous relative[1−3,6] and absolute[4] rate studies of this reaction. The rate of reaction 1 at room temperature is well established. $CH_2ClCH_2CH_2OH$ is generated in the smog chamber via reaction 5. For completeness the rate constant ratios $k(Cl+CH_2ClCH_2CH_2OH)/k_9 = 0.29 \pm 0.02$ and $k(Cl+CH_2ClCH_2CH_2OH)/k_{10} = 0.79 \pm 0.05$ were determined leading to a value of $k(Cl+CH_2ClCH_2CH_2OH) = (7.54 \pm 0.73) \times 10^{-11}$ cm^3 molecule^{-1} s^{-1}.

3.3. Mechanism of the Cl + $CH_3CH_2CH_2OH$ Reaction. The mechanism of the reaction of Cl atoms with $CH_3CH_2CH_2OH$ was investigated by subjecting mixtures of 73−150 mTorr $CH_3CH_2CH_2OH$ and 50−228 mTorr Cl_2 in 700 Torr of N_2 diluent to UV irradiation. The photochemical chain chlorination reactions (1 and 3−5) are expected to lead to formation of the chlorides $CH_3CH_2CHClOH$, $CH_3CHClCH_2OH$, and $CH_2ClCH_2CH_2OH$. The yields of the chlorides provide information on the branching ratio for reaction 1. $CH_2ClCH_2CH_2OH$ is available commercially and a reference spectrum for this species was acquired by introducing known concentrations into the chamber. Neither $CH_3CH_2CHClOH$ nor $CH_3CHClCH_2OH$ is available commercially. By analogy to other α-halogenated alcohols such as CF_3OH,[20] CH_2ClOH,[21] $CHCl_2OH$,[21] CCl_3OH,[21] $CH_3CHClOH$,[22] and $CH_3CCl(OH)CH_3$[23] it is expected that $CH_3CH_2CHClOH$ will undergo decomposition within the smog chamber giving CH_3CH_2CHO and HCl. The decomposition into CH_3CH_2CHO offers a means to calibrate the IR spectrum of $CH_3CH_2CHClOH$.

In the initial experiments using $CH_3CH_2CH_2OH/Cl_2/N_2$, we observed a substantial amount of CH_3CH_2CHO in the spectrum acquired immediately after UV irradiation. There were some IR product features that disappeared when the reaction mixtures were allowed to stand in the dark and some which did not. We ascribe the features that disappeared to $CH_3CH_2CHClOH$. The observation of a substantial yield of CH_3CH_2CHO in the spectrum taken after UV irradiation indicates that for the typical operating conditions of our spectrometer (32 co-added interferograms, 0.25 cm^{-1} resolution, data acquisition time 90 s) there is a significant decomposition of $CH_3CH_2CHClOH$. To capture more of the $CH_3CH_2CHClOH$ within our experimental observation time, we reduced the number of co-added interferograms to 8 and reduced the spectral resolution to 1.0 cm^{-1}. This resulted in a reduction in the data acquisition time from 90 to 11 s. Using this procedure it was possible to monitor the

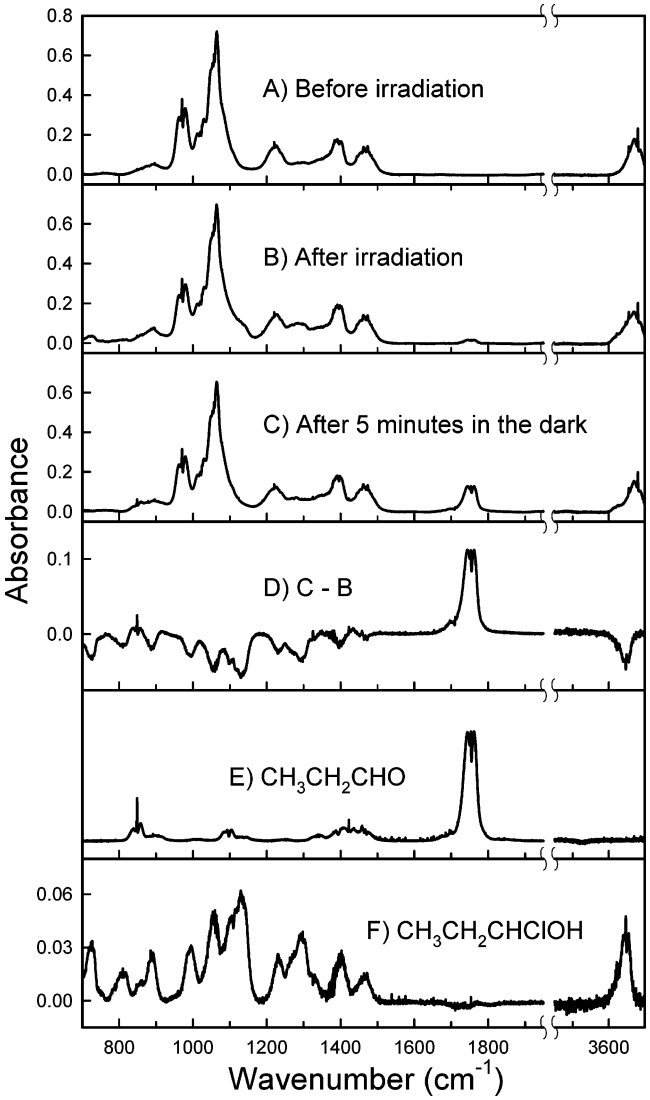

Figure 3. Spectra acquired before (A) and after (B) a 1 s irradiation of a mixture of 73.3 mTorr n-C_3H_7OH and 228 mTorr Cl_2 in 700 Torr of N_2 diluent. Panel C shows the result of leaving the reaction mixture to stand in the dark for 5 min. Comparison of the difference spectrum (D) with a reference spectrum of CH_3CH_2CHO (E) shows the formation of this species. Panel F shows the spectrum of $CH_3CH_2CHClOH$ derived from panel D (see text for details).

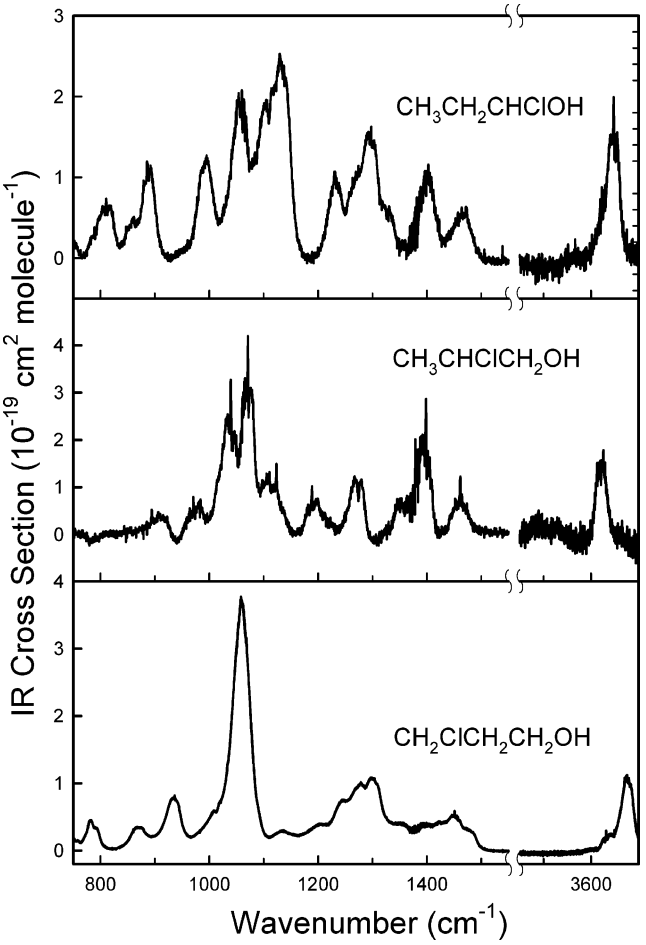

Figure 4. IR spectra of $CH_3CH_2CHClOH$, $CH_3CHClCH_2OH$, and $CH_2ClCH_2CH_2OH$.

decay of $CH_3CH_2CHClOH$ and establish that the decay followed first-order kinetics with a loss rate of $(2.6 \pm 0.3) \times 10^{-2}$ s^{-1}.

Figure 3 shows typical spectra before (A) and after (B) a 1 s irradiation of a reaction mixture containing 73.3 mTorr $CH_3CH_2CH_2OH$ and 228 mTorr Cl_2 in 700 Torr of N_2 diluent. The UV irradiation led to 20% consumption of the $CH_3CH_2CH_2OH$. The result of allowing the product mixture to stand for 5 min in the dark is shown in panel C. Panel D was obtained by subtracting panel B from panel C. Positive features in panel D are attributable to species which are formed when the reaction mixture was left to sit in the dark in the chamber. Negative features in panel D are attributable to species which are lost when the reaction mixture was left to sit in the dark in the chamber. Consistent with expectations outlined above, comparison of panel D with the reference spectrum of CH_3CH_2CHO given in panel E shows this species was formed in the dark. The negative features are then assigned to $CH_3CH_2CHClOH$. Equating CH_3CH_2CHO formation with $CH_3CH_2CHClOH$ loss, we derive the spectrum of $CH_3CH_2CHClOH$ shown in Figure 4. The integrated cross section for $CH_3CH_2CHClOH$ features in the range 650−1650 cm^{-1} was 5.64×10^{-17} cm $molecule^{-1}$ (with an uncertainty estimated to be ±15%). After subtracting IR features attributable to $CH_3CH_2CH_2OH$, $CH_3CH_2CHClOH$, $CH_2ClCH_2CH_2OH$, and CH_3CH_2CHO from panel B, there were residual features at 1039, 1071, 1392, and 3620 cm^{-1} that we attribute to the presence of $CH_3CHClCH_2OH$. Figure 4 shows IR spectra for $CH_3CH_2CHClOH$, $CH_3CHClCH_2OH$, and $CH_2ClCH_2CH_2OH$ derived in the present work. The integrated cross sections for $CH_3CHClCH_2OH$ and $CH_2ClCH_2CH_2OH$ features in the range 650−1650 cm^{-1} were 4.40×10^{-17} and 4.50×10^{-17} cm $molecule^{-1}$, respectively (with an uncertainty estimated to be ±15%).

Figure 5 shows the observed formation of $CH_2ClCH_2CH_2OH$ and CH_3CH_2CHO versus loss of $CH_3CH_2CH_2OH$ following the UV irradiation of $CH_3CH_2CH_2OH/Cl_2/N_2$ mixtures. The data plots are linear indicating the absence of unwanted secondary reactions. The lines through the data are linear least-squares fits which give $k_{1a}/k_1 = 0.60 \pm 0.05$ and $k_{1c}/k_1 = 0.15 \pm 0.03$ and hence we infer $k_{1b}/k_1 = 0.25 \pm 0.08$.

Cheema et al.[6] have studied the products of the Cl atom initiated oxidation of *n*-propanol in 700 Torr of air in the presence of NO at 298 K. Cheema et al.[6] assumed a mechanism for *n*-propanol oxidation and deduced branching ratios of $k_{1a}/k_1 = 0.56$, $k_{1b}/k_1 = 0.30$, and $k_{1c}/k_1 = 0.14$ from the observed yields of HCHO, CH_3CHO, and C_2H_5CHO. The results from the present, more direct study, are in excellent agreement with those of Cheema et al.[6] Given the excellent agreement between these two different approaches it appears that the branching ratios for reaction 1 can be considered to be well established.

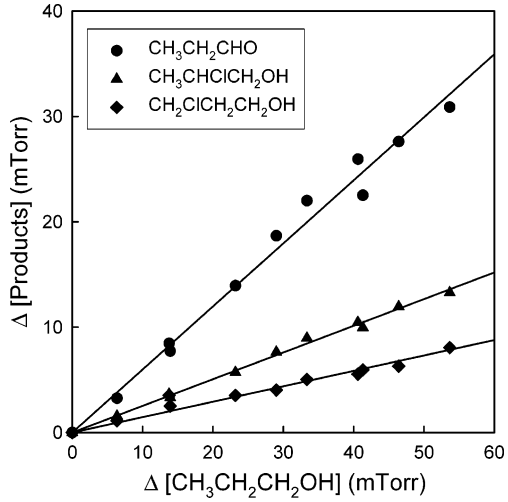

Figure 5. Formation of CH_3CH_2CHO (circles), $CH_3CHClCH_2OH$ (triangles), and $CH_2ClCH_2CH_2OH$ (diamonds) versus *n*-C_3H_7OH loss following the UV irradiation of *n*-C_3H_7OH /Cl_2/N_2 mixtures.

3.4. Theoretical Analysis of Chloropropanol Vibrational Spectra. As further confirmation of the experimental vibrational assignments, we undertook ab initio MP2/6-31G** calculations of the vibrational spectra of the three monochloropropanol geometric isomers. We were initially surprised to find rather poor agreement in number and location of vibrational features between simulation and experiment. Resolution of these discrepancies requires a careful analysis of conformational isomerization in each geometric isomer.

Each geometric isomer contains two C−C and one C−OH rotatable bonds. We expect three local minima when rotating about any one bond, for a total of 27 possible conformers associated with each geometric isomer. Rotations about the $CH_3-CH_2CHClOH$ and $CH_3-CHClCH_2OH$ bonds do not contribute unique conformers; thus up to nine symmetry-distinct conformers are possible for these two geometric isomers. Using Newman projections, the dihedral angles for each isomer are defined as shown in Figure 6, and local minima are labeled

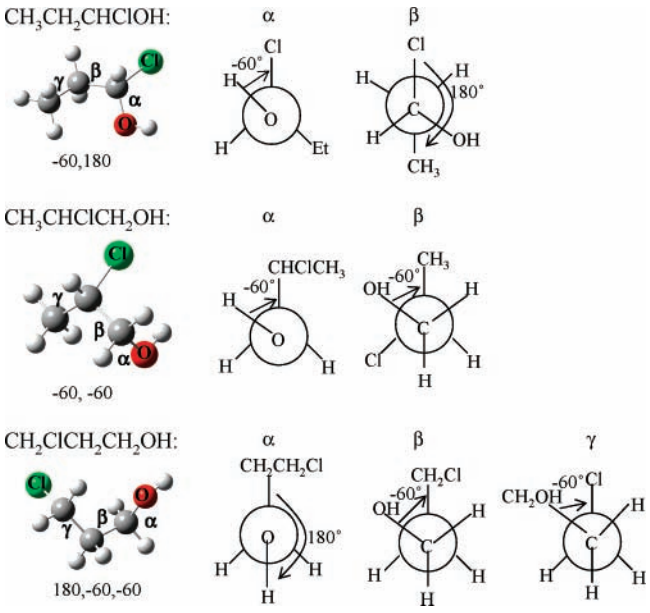

Figure 6. Newman projections of three geometric isomers. α, *β*, and *γ* represent three dihedral angles for three bonds, including two C−C and one C−OH bonds, along the backbone. Thus, for instance, 180,−60,−60 represents a conformer with α of 180°, *β* of −60°, and *γ* of −60°.

−60, 60, and 180°. We calculated the energy-minimized structures, energies, and vibrational spectra of all unique conformers at the MP2/6-31G** level, and the zero-point corrected relative energies are plotted in Figure 7, labeled by approximate dihedral angle values. Conformer energies span a range of up to 20 kJ mol^{-1}, indicating that at room temperature the vibrational spectrum of each isomer will include contributions from multiple conformers.

The lowest energy conformation of $CH_3CHClCH_2OH$ is shown in Figure 6. Sterics clearly do not drive the preference for this conformation: about the HO−CC bond (dihedral α), hydrogen prefers to be gauche to carbon, and similarly about the (HO)C−CHCl(CH_3) bond (dihedral *β*), the OH group prefers to be gauche to both Cl and methyl groups. This particular conformation brings hydroxyl hydrogen and Cl nearby (OH•• •Cl distance = 2.69 Å), facilitating a favorable intramolecular hydrogen bonding interaction:

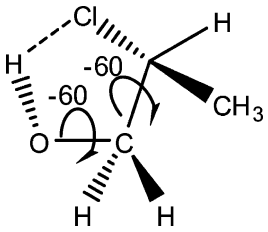

Rotation from this particular gauche,gauche, or "(−60,−60)," conformation about either bond destroys this interaction and leads to higher-energy conformations. For instance, rotation about the C−C bond to place Cl and OH groups trans to one another, conformation (−60,60), costs nearly 7 kJ mol^{-1}. Continuing rotation to (−60,180) brings an oxygen lone pair close to chlorine, increasing the energy further to 13 kJ mol^{-1} above the ground configuration. These three types of relationships between hydroxyl group and chlorine, hydrogen-bonded OH···Cl, trans separated, and repulsive HO···Cl, divides the conformational energy spectrum into three distinct groups (Figure 7). The intermediate energy, or OH trans to Cl, group includes three conformations that are energetically similar. The high-energy grouping includes four conformations with gauche OH and Cl groups with colliding lone pairs.

The low-energy $CH_3CHClCH_2OH$ group includes, in addition to the (−60,−60) conformation, a second one, (60,180), in which OH and Cl are similarly gauche and oriented to facilitate hydrogen bonding (OH···Cl distance = 2.65 Å):

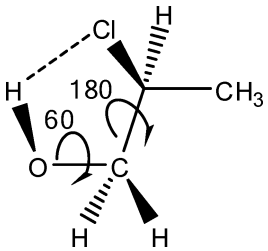

Interconversion between these two low-energy conformers entails rotations about both bonds and that must pass through at least some of the higher energy conformations. One plausible path, for instance, rotates about the C−O bond from (−60,−60) to (−60,60), which costs 6.5 kJ mol^{-1}, about the C−C bond from (−60,60) to the nearly isoenergetic (60,60), and again about the C−O bond to (60,180). Each of these rotations has some intrinsic activation energy, but from this conformational analysis, 6.5 kJ mol^{-1} is a lower bound on the overall activation

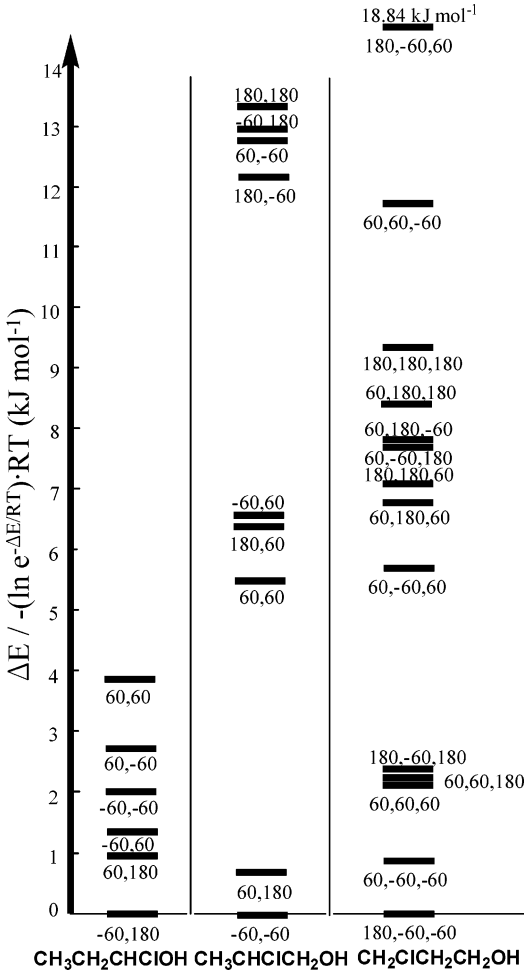

Figure 7. Zero-point corrected MP2/6-31G(d,p) conformer energies (ΔE) relative to most stable conformer of each geometric isomer. The ZPE corrected energies of the ground conformers are are −652.78402082, −652.77961722, and −652.7737268 au, respectively.

energy. Using a typical prefactor of 10^{11} s^{-1}, the rate of interconversion at 296 K is, at most, on the order of 10^{10} s^{-1}.

The interconversion between these two conformations is slow enough to make them distinguishable within the observed vibrational spectrum. We constructed a composite computed vibrational spectrum, shown in the bottom panel of Figure 8, by Lorentz broadening the individual spectra and 296 K Boltzmann weighting according to their corresponding zero-point-corrected energies. Comparison of this composite with the observed spectrum, middle panel of Figure 4, shows very satisfactory agreement in location and intensity of vibrational features. The two lowest energy conformers account for more than 90% of the thermal population of conformers, and we compare the calculated spectra of these individually with that of the composite in Figure 8. The spectra of the two conformers are clearly different, and both contribute unique features to the composite spectrum. For instance, the most intense pair of peaks, labeled 1 and 2 in Figure 8, are clearly distinguished in the experimental spectrum, Figure 4. They correspond to a composite mode and a C−O stretch vibrational mode in the (−60,−60) and (60,180) conformers, respectively. In fact, interconversion of the two conformers is slow enough that rotational fine structure on these two modes can be distinguished in the observed spectrum. Similarly, the feature near 1300 cm^{-1} corresponds to the Cl−C−O bend in the two conformers, labeled 4 and 5 in Figure 8, and the feature near 1400 cm^{-1} is a composite of peaks 6 and 8 from the two. The O−H stretch near 3600 cm^{-1} is predicted to be split by 40 cm^{-1}, as is barely discernible in the observed spectrum. The strong conformational isomerism in $CH_3CHClCH_2OH$ is thus clearly distinguished in its vibrational spectrum.

All three dihedral angles contribute to conformational isomerization in $CH_2ClCH_2CH_2OH$. Unlike $CH_3CHClCH_2OH$, this geometric isomer has no chiral centers, so that mirror image conformers are not energetically or structurally distinct from one another. As a result, $CH_2ClCH_2CH_2OH$ has 14 distinct conformers, 13 of which possess degenerate mirror images in which the dihedral angles about all bonds are reversed (e.g., conformers denoted (180,−60,−60) and (180,60,60) are identical mirror images), and one of which, corresponding to 180° dihedrals about all three rotatable bonds, has C_s symmetry and is its own mirror image. The lowest energy conformer is shown in Figure 6, and the energies of other conformers relative to this baseline shown in Figure 7. As observed for $CH_3CHClCH_2$-OH, hydrogen OH···Cl hydrogen bonding has a large influence on conformational stability, but in this case this interaction is convoluted with hydrogen bonding between oxygen and an acidic hydrogen on the terminal carbon:

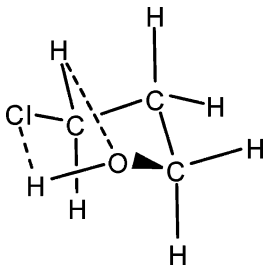

The OH···Cl and HO···HC distances in the lowest energy (180,−60,−60) conformer are 2.86 and 2.50 Å, respectively, and adopt similar values (2.87 and 2.59) in the nearly isoenergetic (60,−60,−60) conformer. Within 2 kJ mol^{-1} of these two are three more conformers that retain the HO···HC interaction but lose the OH···Cl one. At somewhat higher energy are conformers that lack hydrogen bonding and at the top of the energy scale are conformers in which chlorine and hydroxyl oxygen are brought into close proximity without the intervention of an H bond.

From a Boltzmann analysis, all five of the lowest energy conformations contribute significantly to the equilibrium composition and to the observed vibrational spectrum. The calculated composite spectrum is shown in the bottom panel of Figure 9 and can be compared with the observed spectrum in Figure 4. Again, agreement between the two is generally good. The composite spectrum does contain a number of distinct features, for instance a H−C−O−H bend mode (peak 1) is observed at 1220 cm^{-1} in (180,−60,−60). The circled peaks are from other high-energy configurations. The 1250−1400 cm^{-1} regime is broadened and indistinct in the observed spectrum. We attribute this broadening to relatively rapid interconversion of the low-energy conformers. All five are related by simple rotations about bonds, and each conformer can be reached by a path that does not pass through any of the higher energy conformations. The barriers to rotation are thus expected to be lower and lifetimes of the individual conformers shorter than those in the CH_3-$CHClCH_2OH$ case, producing a broadened spectrum that blurs the individual conformational contributions.

$CH_3CH_2CHClOH$ differs from the other two geometric isomers in that both electronegative groups are attached to the same carbon center. Because this carbon is chiral, we might expect the isomer to exhibit nine stable conformers (Figure 6).

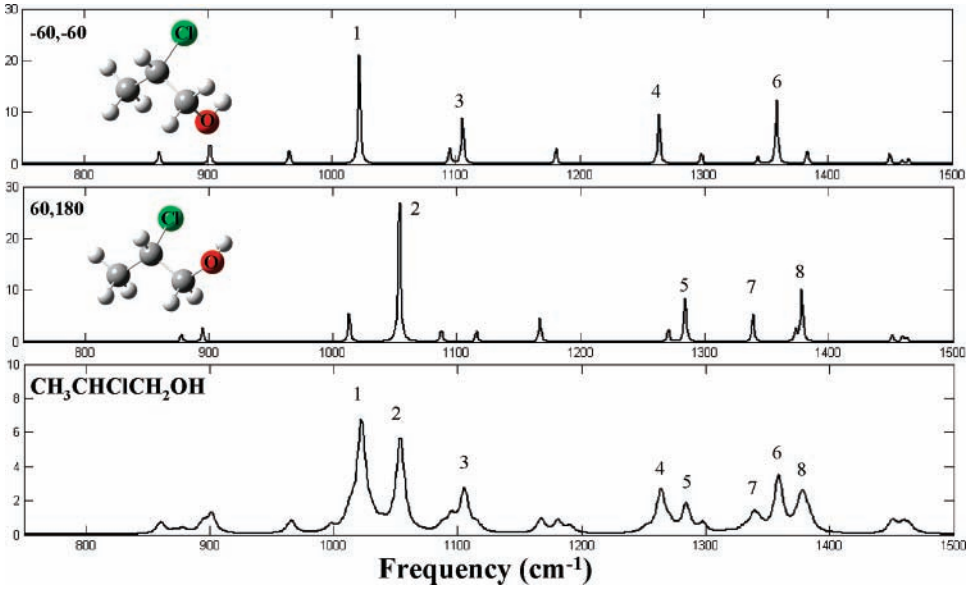

Figure 8. Calculated IR spectra of two lowest-energy $CH_3CHClCH_2CH_2OH$ conformers and Boltzmann-weighted composite spectrum of all conformers. Numbered peaks indicate correspondence between composite spectrum and distinct conformer modes.

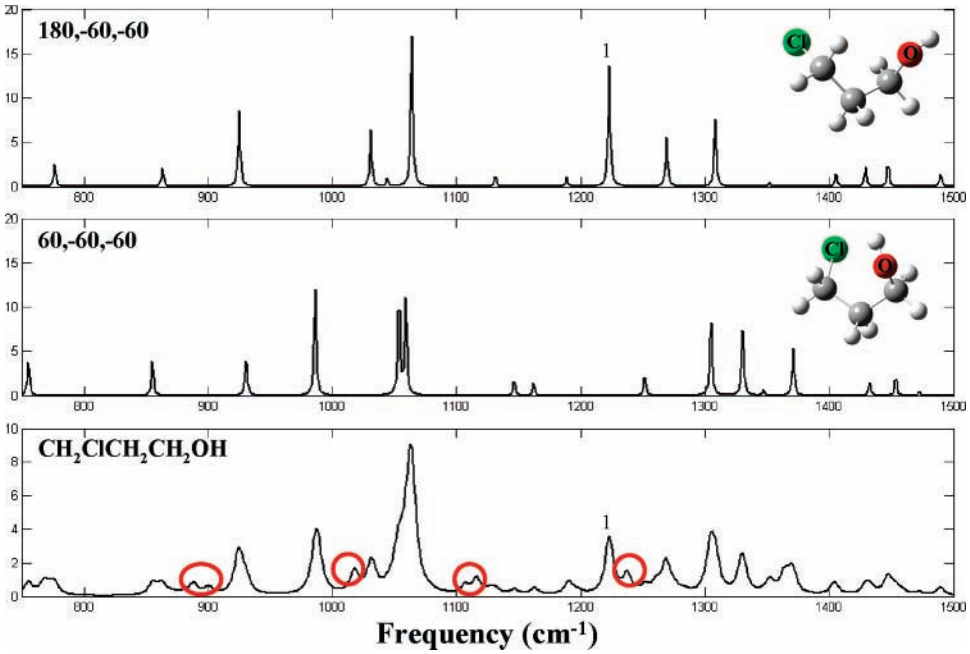

Figure 9. Calculated IR spectra of two lowest-energy $CH_2ClCH_2CH_2OH$ conformers and Boltzmann-weighted composite spectrum of all conformers. Numbered peaks indicate correspondence between composite spectrum and distinct conformer modes. Circles indicate contributions from higher energy conformations.

Three of these conformations, corresponding to a trans orientation about the HO−CCl fragment, are energetically unstable. To confirm this result, we performed a potential energy scan about this bond, holding its dihedral angle fixed, orienting the OC−CC dihedral angle β near 180°, and allowing all degrees of freedom other than the α dihedral to relax. As shown in Figure 10, both gauche orientations of the OH group relative to Cl are stable, while the trans conformer is near an energy maximum. Transition state optimization identifies a barrier of 20 kJ mol^{-1} at an angle of 33°, while the two gauche conformers are separated by a barrier of 10.4 kJ mol^{-1}. This behavior is similar to that found for halogenated methanols[25] and reflects the influence of negative hyperconjugation between electronegative groups that imparts partial double bond character on the C−O bond:

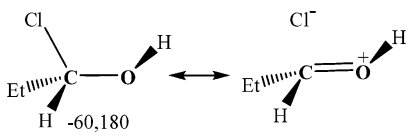

Electron-withdrawing Cl promotes partial conjugation between O loan pairs and the C center, but this conjugation is lost when H is trans to Cl. The lowest energy conformer, shown in Figure 6, has H trans to ethyl and Cl trans to methyl (β of 180). Rotating about C−OH to place H gauche to both Cl and ethyl

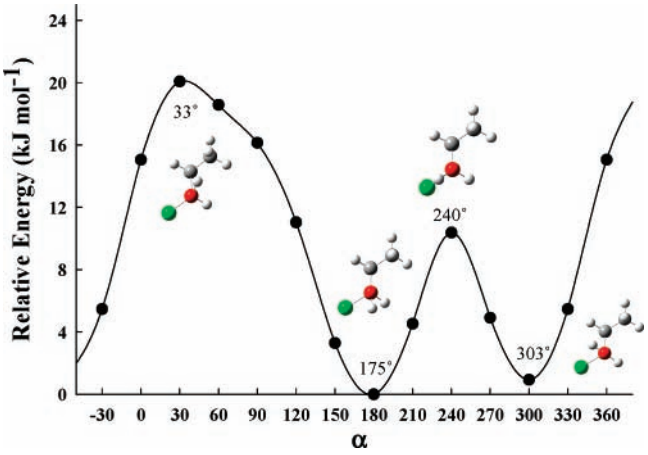

Figure 10. Potential energy surface of conformers (α,180) for $CH_3CH_2CHClOH$. We note that non-restricted geometry optimization was carried out when α was at 180°, 240°, and 300°, while restricted optimization was performed for other angles by fixing α. Numbers by the curve indicate the values of α after full optimization.

increases the conformational energy about 1 kJ mol^{-1}, and other combinations about the two bonds are up to several kJ mol^{-1}.

From the Boltzmann analysis, all six conformers have significant populations at 296 K and contribute to the observed vibrational spectrum. The bottom panel of Figure 11 shows the composite vibrational spectrum, and comparison with the top panel of Figure 4 again indicates very good agreement between observation and calculation. Because of slow interconversion induced by negative hyperconjugation about the HO−CCl bond, contributions from different conformers are clearly distinguishable in the observed spectrum. We compare the calculated spectra of these individually with that of the composite in Figure 11. For instance, peak 1 at 1260 cm^{-1} belongs to the (−60,-180) conformer. The CH_2 wag mode ($CH_3-CH_2-CHClOH$) is observed at 1320 cm^{-1} (peak 2) in (−60, 180) and 1335 cm^{-1} (peak 4) in (60,180), respectively. Peaks at 1200 cm^{-1} (peak 5) and 1300 cm^{-1} (peak 6) represent H−C−O−H bend and H−C−O bend in (−60,60). Clearly, the circled features represent contributions from other higher energy conformers. For example, the C−O stretch at 1100 cm^{-1} is from (−60,−60). This analysis further confirms that all the configurations contribute significantly to the composed spectrum due to small energy difference from one another and that they interconvert slowly on the time scale of the spectroscopic experiment.

As is common for alpha halogenated alcohols, $CH_3CH_2CHClOH$ is observed to decompose in the smog chamber to propanal and HCl. Consistent with results reported previously for 2-chloro-2-propanol, we calculate homogeneous decomposition via direct HCl elimination to be endothermic by 20 kJ mol^{-1}, to have a free energy of decomposition of −18 kJ mol^{-1}, and an activation energy of 137 kJ mol^{-1} at 0 K. While HCl elimination is clearly thermodynamically driven, homogeneous decomposition cannot account for the rapid loss observed; heterogeneous processes most likely account for this decomposition.

4. Discussion

The results from the present work confirm the literature value of k_1 and provide measurements of the branching ratios k_{1a}/k_1, k_{1b}/k_1, and k_{1c}/k_1 which are consistent with, but more direct than, the single previous measurement. Using the data presented in the present work we can calculate site specific rate constants

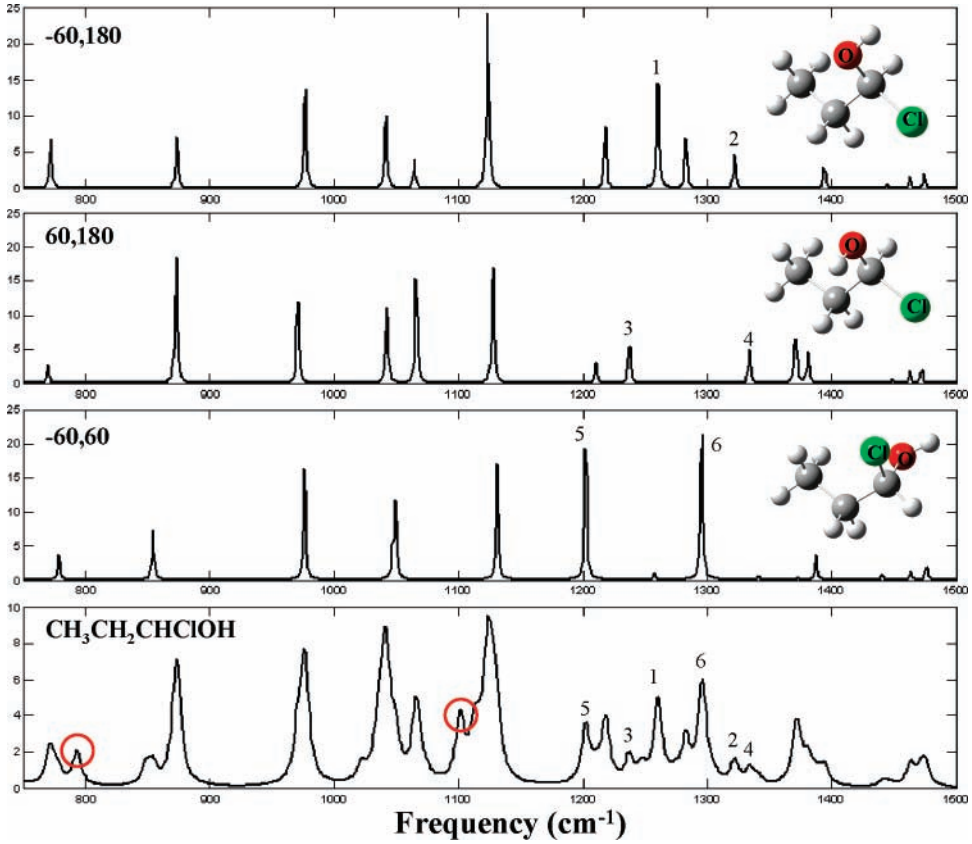

Figure 11. Calculated IR spectra of three lowest-energy $CH_3CH_2CHClOH$ conformers and Boltzmann-weighted composite spectrum of all conformers. Numbered peaks indicate correspondence between composite spectrum and distinct conformer modes. Circles indicate contributions from higher energy conformations.

of $k_{1a} = (1.04 \pm 0.13) \times 10^{-10}$, $k_{1b} = (4.35 \pm 1.44) \times 10^{-11}$, and $k_{1c} = (2.61 \pm 0.57) \times 10^{-11}$ cm^3 molecule^{-1} s^{-1}. We can compare k_{1c} with the reactivity of Cl atoms toward $-CH_3$ groups in C_2H_6, 2.95×10^{-11}; C_3H_6, 3.05×10^{-11}; and n-C_4H_{10}, 3.02×10^{-11} cm^3 molecule^{-1} s^{-1}.[26] The reactivity of the $-CH_3$ group in *n*-propanol is indistinguishable from that in alkanes indicating that the presence of the $-$OH group does not impact the reactivity of the 3°-substituents substantially. Comparing k_{1a} and k_{1b} with the reactivity of Cl atoms toward $-CH_2-$ groups in C_3H_6 (7.74×10^{-11}) and *n*-C_4H_{10} (7.29×10^{-11}) it is evident that the $-$OH group activates the 1° position with respect to attack by Cl atoms and deactivates the 2° position. The present work together with previous studies of *n*-propanol,[5] *i*-propanol,[23] and ethanol[22] indicate that in reactions of Cl atoms with alcohols, the $-$OH group activates the 1° position, deactivates the 2° position, and has little influence on the 3° position.

The chlorinated *n*-propanols have rich and individually unique conformational chemistries that are clearly discernible in the observed vibrational spectra. Such effects are not as evident in the vibrational spectra of even the closely related chlorinated *i*-propanols.[23] Intramolecular hydrogen bonding favors two conformers of $CH_3CHClCH_2OH$ over the remaining seven and introduces an appreciable barrier to interconversion. These two dominate the observed spectrum and contribute clearly distinguishable unique vibrational features. Hydrogen-bonding similarly dominates the conformations of $CH_2ClCH_2CH_2OH$, but here the larger number and easier interconversion of isomers produces the observed broadened and feature-poor spectrum. Negative hyperconjugation limits $CH_3CH_2CHClOH$ to only six stable conformers of similar energy, but slow interconversion allows these to be distinguished spectroscopically. Similar effects are present in other halogenated alcohols: such isomerization has been detected in the vibrational spectrum of 2-chloroethanol[8] and 2-fluoroethanol.[9]

Finally, we calculate that as with other 1°-chloroalcohols[21] there is a substantial barrier for homogeneous decomposition of $CH_3CH_2CHClOH$. The calculation shows a low rate ($<1.0 \times 10^{-11}$ s^{-1}) of homogeneous elimination of HCl, which is much slower than the rate of approximately 10^{-2} s^{-1} implied by the approximately 1 min lifetime observed experimentally. While homogeneous gas-phase decomposition of α-chloroalcohols appears to be of negligible importance, heterogeneous decomposition is likely to be a significant atmospheric loss mechanism for these species.

Acknowledgment. The authors thank Josh Bruce and Shawn Coleman for assistance with construction of the vibrational spectra. W.F.S. and L.X. thank Ford Motor Co. for support of this work.

References and Notes

(1) Wallington, T. J.; Skewes, L. M.; Siegl, W. O.; Wu, C.-H.; Japar, S. M. *Int. J. Chem. Kinet.* **1988**, *20*, 867.

(2) Nelson, L.; Rattigan, O.; Neavyn, R.; Sidebottom, H.; Treacy, J.; Nielsen, O. J. *Int. J. Chem. Kinet.* **1990**, *22*, 1111.

(3) Wu, H.; Mu, Y.; Zhang, X.; Jiang, G. *Int. J. Chem. Kinet.* **2003**, *35*, 81.

(4) Taketani, F.; Takahashi, K.; Matsumi, Y.; Wallington, T. J. *J. Phys. Chem. A* **2005**, *109*, 3955.

(5) Garzón, A.; Cuevas, C. A.; Ceacero, A. A.; Notario, A.; Albaladejo, J.; Fernández-Gómez, M. *J. Chem. Phys.* **2006**, *125*, 104305.

(6) Cheema, S. A.; Holbrook, K. A.; Oldershaw, G. A.; Walker, R. W. *Int. J. Chem. Kinet.* **2001**, *34*, 110.

(7) NIST Standard Reference Database 25, Structures and Properties, Version 2.02; National Institute for Standards and Technology: Gaithersburg, MD, 1994.

(8) Durig, J. R.; Zhou, L.; Gounev, T. K.; Klaeboe, P.; Guirgis, G. A.; Wang, L. *J. Mol. Struct.* **1996**, *385*, 7.

(9) Bakke, J. M.; Bjerkeseth, L. H.; Rønnow, T. E. C. L.; Steinsvoll, K. *J. Mol. Struct.* **1994**, *321*, 205.

(10) Hoffmann, R.; Radom, L.; Pople, J. A.; Schleyer, P. v. R.; Hehre, W. J.; Salem, L. *J. Am. Chem. Soc.* **1972**, *94*, 6221.

(11) Wallington, T. J.; Japar, S. M. *J. Atmos. Chem.* **1989**, *9*, 399.

(12) Frisch, M. J.; Trucks, G. W.; Schlegel, H. B.; Scuseria, G. E.; Robb, M. A.; Cheeseman, J. R.; Montgomery, J. A., Jr.; Vreven, T.; Kudin, K. N.; Burant, J. C.; Millam, J. M.; Iyengar, S. S.; Tomasi, J.; Barone, V.; Mennucci, B.; Cossi, M.; Scalmani, G.; Rega, N.; Petersson, G. A.; Nakatsuji, H.; Hada, M.; Ehara, M.; Toyota, K.; Fukuda, R.; Hasegawa, J.; Ishida, M.; Nakajima, T.; Honda, Y.; Kitao, O.; Nakai, H.; Klene, M.; Li, X.; Knox, J. E.; Hratchian, H. P.; Cross, J. B.; Bakken, V.; Adamo, C.; Jaramillo, J.; Gomperts, R.; Stratmann, R. E.; Yazyev, O.; Austin, A. J.; Cammi, R.; Pomelli, C.; Ochterski, J. W.; Ayala, P. Y.; Morokuma, K.; Voth, G. A.; Salvador, P.; Dannenberg, J. J.; Zakrzewski, V. G.; Dapprich, S.; Daniels, A. D.; Strain, M. C.; Farkas, O.; Malick, D. K.; Rabuck, A. D.; Raghavachari, K.; Foresman, J. B.; Ortiz, J. V.; Cui, Q.; Baboul, A. G.; Clifford, S.; Cioslowski, J.; Stefanov, B. B.; Liu, G.; Liashenko, A.; Piskorz, P.; Komaromi, I.; Martin, R. L.; Fox, D. J.; Keith, T.; Al-Laham, M. A.; Peng, C. Y.; Nanayakkara, A.; Challacombe, M.; Gill, P. M. W.; Johnson, B.; Chen, W.; Wong, M. W.; Gonzalez, C.; Pople, J. A. *Gaussian 03*, revision C.02; Gaussian, Inc.: Wallingford, CT, 2004.

(13) Scott, A. P.; Radom, L. *J. Phys. Chem.* **1996**, *100*, 16502.

(14) Adams, M. J. *Chemometrics in Analytical Spectroscopy*, 2nd ed.; The Royal Society of Chemistry: Cambridge, 2004.

(15) Atkinson, R.; Aschmann, S. M. *Int. J. Chem. Kinet.* **1985**, *17*, 33.

(16) Wallington, T. J.; Skewes, L. M.; Siegl, W. O. *J. Photochem. Photobiol. A: Chem.* **1988**, *25*, 167.

(17) Kaiser, E. W.; Wallington, T. J. *J. Phys. Chem.* **1996**, *100*, 9788.

(18) Wallington, T. J.; Andino, J. M.; Lorkovic, I. M.; Kaiser, E. W.; Marston, G. *J. Phys. Chem.* **1990**, *94*, 3644.

(19) Ezell, M. J.; Wang, W.; Ezell, A. A.; Soskin, G.; Finlayson-Pitts, B. J. *Phys. Chem. Chem. Phys.* **2002**, *4*, 5813.

(20) Sehested, J.; Wallington, T. J. *Environ. Sci. Tech.* **1993**, *27*, 146.

(21) Wallington, T. J.; Schneider, W. F.; Barnes, I.; Becker, K. H.; Sehested, J.; Nielsen, O. J. *Chem. Phys. Lett.* **2000**, *322*, 97.

(22) Taatjes, C. A.; Christensen, L. K.; Hurley, M. D.; Wallington, T. J. *J. Phys. Chem. A* **1999**, *103*, 9805.

(23) Yamanaka, T.; Kawasaki, M.; Hurley, M. D.; Wallington, T. J.; Schneider, W. F. *Phys. Chem. Chem. Phys.* **2007**, *9*, 4211.

(24) Schneider, W. F.; Nance, B. I.; Wallington, T. J. *J. Am. Chem. Soc.* **1995**, *117*, 478.

(25) Atkinson, R.; Baulch, D. L.; Cox, R. A.; Crowley, J. N.; Hampson, R. F., Jr.; Jenkin, M. E.; Kerr, J. A.; Rossi, M. J.; Troe, J. IUPAC Subcommittee on Gas Kinetic Data Evaluation, http://www.iupac-kinetic-.ch.cam.ac.uk/index.html, downloaded August 2006.